Applied Catalysis B: Environmental 142–143 (2013) 744–751

Contents lists available at SciVerse ScienceDirect

Applied Catalysis B: Environmental

journal homepage: www.elsevier.com/locate/apcatb

Hierarchical porous AgCl@Ag hollow architectures: Self-templating synthesis and highly enhanced visible light photocatalytic activity

Lunhong Ai, Caihong Zhang, Jing Jiang*

Chemical Synthesis and Pollution Control Key Laboratory of Sichuan Province, College of Chemistry and Chemical Engineering, China West Normal University, Nanchong 637002, PR China

ARTICLE INFO

Article history:
Received 1 March 2013
Received in revised form 27 April 2013
Accepted 22 May 2013
Available online 31 May 2013

Keywords:
Photocatalysis
AgCl
Silver
Surface plasmon resonance
Templating synthesis

ABSTRACT

Hierarchical porous AgCl@Ag hollow architectures (HAs) were successfully synthesized by a facile, inexpensive and scalable approach through template-engaged acidic etching of uniform Ag_2CO_3 architectures at room temperature. The critical surface chlorination and pore creation were realized by using NH_4Cl as a reactive acidic etching agent. The samples were characterized by X-ray diffraction (XRD), scanning electron microscopy (SEM), energy-dispersive spectroscopy (EDS), X-ray photoelectron spectroscopy (XPS), and UV–vis diffuse reflectance spectroscopy (DRS). The results showed that the products were composed of large amounts of polyhedron with hollow interior and porous surface. The as-synthesized AgCl@Ag HAs exhibited remarkable photocatalytic activity and excellent durability for the degradation of organic pollutants under visible light irradiation. The photocatalytic reaction followed the pseudo-first-order kinetics and the rate constant for the degradation of methyl orange (MO) photocatalyzed by AgCl@Ag HAs was 1.6 times that of the solid counterparts. The enhanced photocatalytic activity could be attributed to the hierarchical hollow morphology and unique porous structure, providing increased adsorption and enhanced light-harvesting efficiency.

1. Introduction

Heterogeneous photocatalysis for solar harnessing and converting is of great importance for the development of the sustainable environment and energy, which have stimulated intense research interest in recent years [1,2]. A semiconductor photocatalyst absorbs incident photons with energy higher than its band gap to transfer the light energy into chemically useful charge carriers, subsequently driving redox reactions at the surface of photocatalyst. Undoubtedly, the light harvesting of photocatalysts that directly dominates the generation of active redox charge carriers is a critical issue for manipulating the photocatalytic performance. The metal oxide semiconductors such as TiO_2 and ZnO with considerable photoreactivity and photostability are the most extensively used materials in semiconductor photocatalysis [3,4]. However, limited light absorption region of these semiconductors often results in the low efficiencies of light utilization and low rates of photochemical processes. On the other hand, as for many photochemical process only a very small partial incident photons is actually harvested and then converted to chemical energy by semiconductor photocatalysts, because of the existed large loss stemmed from inevitable scattering, transmission and heat conversion during light transportation in the medium [5]. Therefore, it is essential to design suitable structures to help trap/absorb more incident light and achieve cooperatively enhanced photocatalytic performances.

The porous hierarchical architectures have attracted great research interest in the field of photocatalysis in recent years, due to their extraordinary textural characteristics, well-defined morphology, structural flexibility, and chemical stability. In particular, compared to solid counterparts, porous structure with hollow interiors can accommodate a large number of guest molecules producing some strange microcosmic "package" effect, provide multiple accessible channels for transport of the reactants shortening the diffusion paths to active surface sites, and allow light scattering within the interior cavity to promote the light-harvesting efficiency. To this end, the porous hierarchical hollow architectures have emerged as an ideal choice for the design and fabrication of the highly active photocatalysts. For example, Pan et al. reported a self-etching synthesis of porous F-containing TiO_2 hollow microspheres with excellent performances in photocatalysis [6]. Huang et al. explored an anion exchange strategy for the synthesis of Bi_2WO_6 hollow microspheres displaying high gas adsorption capacity and photocatalytic reduction activity [7]. In addition, other semiconductors such as WO_3 [8], Fe_2O_3 [9], BiOI [10], $Bi_4V_2O_{11}$ [11] and Ag_2ZnGeO_4 [12] were successfully synthesized in the form of hierarchical hollow structures. Very recently, Bi_2O_3/Bi_2WO_6 composites with hollow interior have been prepared via a templated method, which also exhibited the enhanced photocatalytic activity

* Corresponding author. Tel.: +86 817 2568081; fax: +86 817 2582029.
E-mail address: 0826zjjh@163.com (J. Jiang).

0926-3373/$ – see front matter © 2013 Elsevier B.V. All rights reserved.
http://dx.doi.org/10.1016/j.apcatb.2013.05.053

[13]. Therefore, shaping and structure-engineering not only is an exciting direction to pursue for highly active photocatalysts but also offers opportunities to investigate the relationship between the structural properties and the photocatalytic properties.

Recently, the silver/silver chloride (denoted as AgCl@Ag) have attracted considerable attention as a promising photocatalyst working under visible light for pollutant degradation [14,15], water disinfection [16], and carbon dioxide reduction [17], due to the remarkable surface plasmon resonance (SPR) effect of metallic silver nanoparticles (NPs). Huang et al. synthesized AgCl@Ag plasmonic photocatalysts by an ion-exchange reaction, followed by photoreduction in the presence of methyl orange (MO) [14]. Sun et al. reported a thermal polyol process to synthesize cubic AgCl@Ag plasmonic photocatalysts [18]. Chen et al. fabricated quasicubic and spherical AgCl@Ag plasmonic photocatalyst by a surfactant-assisted method in an oil-in-water system [19]. Our group also developed a microwave nonaqueous method to synthesize daylight-driven triangular pyramid AgCl@Ag plasmonic photocatalysts [20]. Despite these advances, the realization of shaping AgCl@Ag plasmonic photocatalysts with hierarchical porous hollow structures by a facile approach remains a great challenge.

Inspired by our recent sacrificial templating synthesis strategy [21–23], we herein report a facile and rational synthesis of hierarchical porous AgCl@Ag hollow architectures (HAs) by using sacrificial Ag_2CO_3 as template for the first time. This strategy is simple, inexpensive and scalable, and the whole processing is especially at room temperature. In our synthetic strategy, the Ag_2CO_3 architectures function not only as reactive silver source, but also serve as scaffold for creating hollow structures to guide the formation of the AgCl@Ag HAs. More importantly, the as-synthesized AgCl@Ag HAs exhibit greatly enhanced photocatalytic activity for the degradation of MO under visible light. The rate constant for the MO degradation photocatalyzed by AgCl@Ag HAs was 1.6 times that of the solid counterparts. The enhanced photocatalytic activity is attributed to the hierarchical hollow morphology and unique porous structure, which could provide more surface active sites, better permeability and enhanced light-harvesting efficiency.

2. Experimental

2.1. Materials

$AgNO_3$, $NaHCO_3$, NH_4Cl, $Na_2C_2O_4$, isopropyl alcohol, disodiumethylenediamine tetraacetate (EDTA) and methyl orange (MO) were purchased from Kelong Chemical Reagents Company (Chengdu, China) and used without further purification. All chemicals used in this study were of commercially available analytical grade.

2.2. Synthesis of hierarchical porous AgCl@Ag HAs

Sacrificial Ag_2CO_3 templates were first prepared by a facile and mild precipitation process at room temperature. In a typical procedure, 1 mmol of $AgNO_3$ were dissolved in 40 mL of deionized water to form a clear solution, followed by a dropwise addition of 40 mL of $NaHCO_3$ aqueous solution (0.0125 M) under magnetically stirring. The obtained gray yellow precipitates were collected by centrifugation, washed for three times with deionized water, and dried at 60 °C for 6 h. The hierarchical porous AgCl@Ag HAs were fabricated under ambient condition in our laboratory. Typically, 0.05 g of as-obtained Ag_2CO_3 samples were dispersed in 10 mL of deionized water, followed by the addition of NH_4Cl (0.243 g). The mixture was continuously stirred for 40 min at room temperature and collected by centrifugation, washed with deionized water for three times, and dried at 60 °C for 6 h.

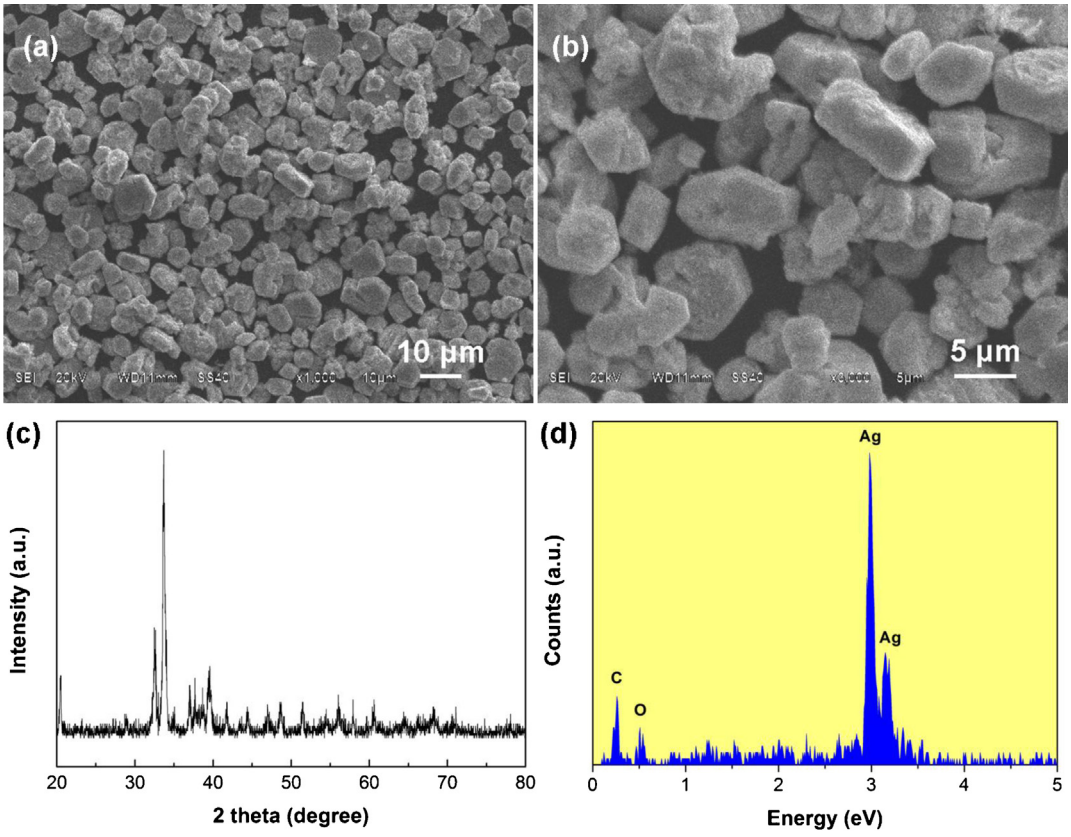

Fig. 1. (a and b) SEM images, (c) XRD pattern and (d) EDS spectrum of Ag_2CO_3 architectures.

2.3. Characterization

The powder X-ray diffraction (XRD) measurements were recorded on a Rigaku Dmax/Ultima IV diffractometer with monochromatized Cu Kα radiation (λ = 0.15418 nm). The morphology was observed with a JEOL JSM-6510LV scanning electron microscope (SEM). The elemental composition of the samples was characterized by energy-dispersive X-ray spectroscopy (EDS, Oxford instruments X-Max). X-ray photoelectron spectroscopy (XPS) measurements were recorded on a Perkin-Elmer PHI 5000C spectrometer using monochromatized Al Kα excitation. All binding energies were calibrated by using the contaminant carbon (C_{1S} = 284.6 eV) as a reference. UV–vis diffused reflectance spectra of the samples were obtained for the dry-pressed film samples using a UV–vis spectrophotometer (UV-3600, Shimadzu, Japan). $BaSO_4$ was used as a reflectance standard in a UV–vis diffuse reflectance experiment.

2.4. Evaluation of photocatalytic activity

The visible-light-driven photocatalytic activity experiments of the AgCl@Ag HAs for the degradation of MO were performed at ambient temperature using a 350 W Xe arc lamp with a 420 nm cutoff filter as the light source. A 0.05 g amount of photocatalyst was added into 100 mL of 10 mg L^{-1} MO aqueous solution in a container. The MO solution with photocatalyst was continuously stirred for 30 min to ensure the establishment of an adsorption–desorption equilibrium before the lamp was turned on. During the degradation, the MO solution with photocatalyst was continuously stirred by a magnetic stirrer and the concentration of MO was monitored by colorimetry with a Shimadzu UV-2550 UV–vis spectrometer.

3. Results and discussion

Ag_2CO_3 architecture templates can be easily and directly prepared by a wet chemical method. Fig. 1a shows a typical SEM image of the Ag_2CO_3 products. It can be seen that the as-synthesized products were composed of a large quantity of uniform particles with distinctively polyhedral morphology. The size of the polyhedral structure was on the scale of micrometers with a diameter of 5–10 μm. The high-magnification SEM image in Fig. 1b revealed that the polyhedral structure presented well-defined facets and smooth exterior surfaces. Fig. 1c displays the typical XRD pattern of the Ag_2CO_3 products. All the diffraction peaks can be readily indexed to a pure, monoclinic crystalline phase Ag_2CO_3, which was in good agreement with the standard card (JCPDS card no. 70-2184), and no diffraction peaks from the impurities were detected. The strong and sharp peaks indicate that the as-prepared Ag_2CO_3 products were well crystallized. Fig. 1d is the energy dispersive spectrum (EDS) of the Ag_2CO_3 products, in which C, O and Ag elements are present together.

Fig. 2a shows the XRD pattern of the AgCl@Ag products prepared by the chemical transformation of the Ag_2CO_3 architectures in the presence of NH_4Cl. The intense diffraction peaks at 2θ of 27.6° (1 1 1), 32.1° (2 0 0), 46.0° (2 2 0), 54.5° (3 1 1), 57.4° (2 2 2), 67.1° (4 0 0), 74.4° (3 3 1) and 76.5° (4 2 0) could be unambiguously detected. These diffraction peaks correspond to the typical cubic phase of AgCl (JCPDS file no. 31-1238), revealing the successful phase transformation from monoclinic Ag_2CO_3 to cubic AgCl. Moreover, the additional peaks at 38.2° and 64.8° marked with arrow in Fig. 2a could match with that of the typical cubic phase of metallic Ag (JCPDS no. 65-2871). The low and weak peaks of metallic Ag indicate the low content and/or poor crystallinity of Ag in our sample. The XRD results reflect the coexistence of AgCl and metallic Ag in the AgCl@Ag sample. The element composition of the AgCl@Cl

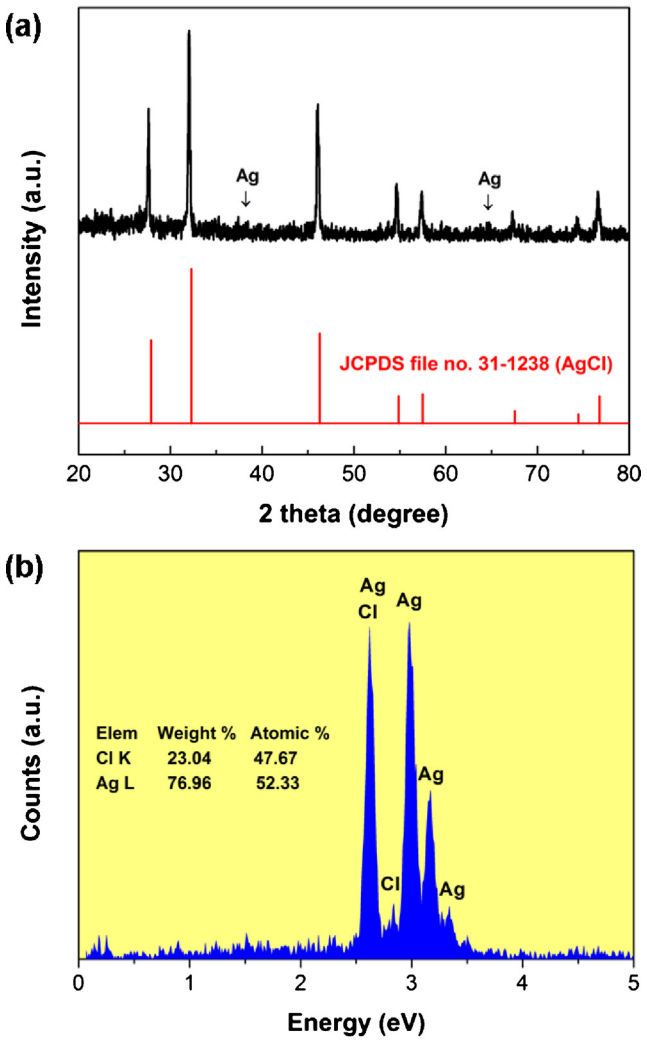

Fig. 2. (a) XRD pattern and (b) EDS spectrum of AgCl@Ag HAs.

sample was identified by EDS analysis (Fig. 2b). The AgCl@Ag sample is composed of Ag and Cl elements, and the quantitative analysis shows that the atomic ratio of Ag to Cl elements is approximately 1.09:1.

The chemical composition and surface chemical states of the AgCl@Ag products were confirmed by X-ray photoelectron spectroscopy (XPS). As shown in Fig. 3a, the AgCl@Ag sample displays double peaks located at 198.0 and 199.5 eV, which can be assigned to the characteristic doublets of Cl $2p_{3/2}$ and Cl $2p_{1/2}$, respectively [24]. The high-resolution spectrum of Ag 3d is shown in Fig. 3b. It could be deconvoluted into two doublets: the one consists of two peaks with binding energies of 366.7 and 372.7 eV, which are assigned to Ag $3d_{3/2}$ and Ag $3d_{5/2}$ of AgCl, respectively; the other has binding energies of 374.1 and 368.1 eV, corresponding to the metallic Ag [25]. The quantitatively calculated surface mole ratio of Ag^+ to Ag^0 in the AgCl@Ag products is approximately 11:1. The XPS analysis combined with above XRD and EDS results solidly verifies the formation of the AgCl@Ag containing of metallic Ag and AgCl together.

Scanning electron microscopy (SEM) further provided insights into the morphology and detailed structure of the AgCl@Ag products. A general view of the product (Fig. 4a) reveals that it was composed of large amounts of polyhedral structure, suggesting that the architectures were maintained for the AgCl@Ag product during

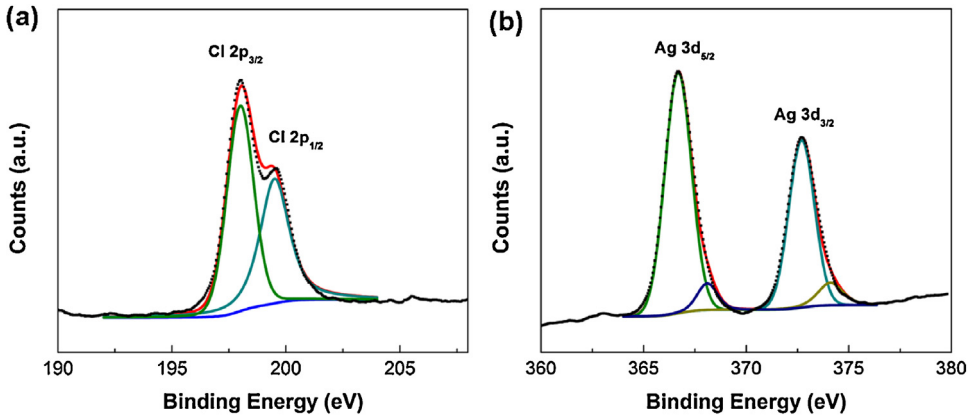

Fig. 3. XPS spectra of (a) Cl 2p and (b) Ag 3d of AgCl@Ag HAs.

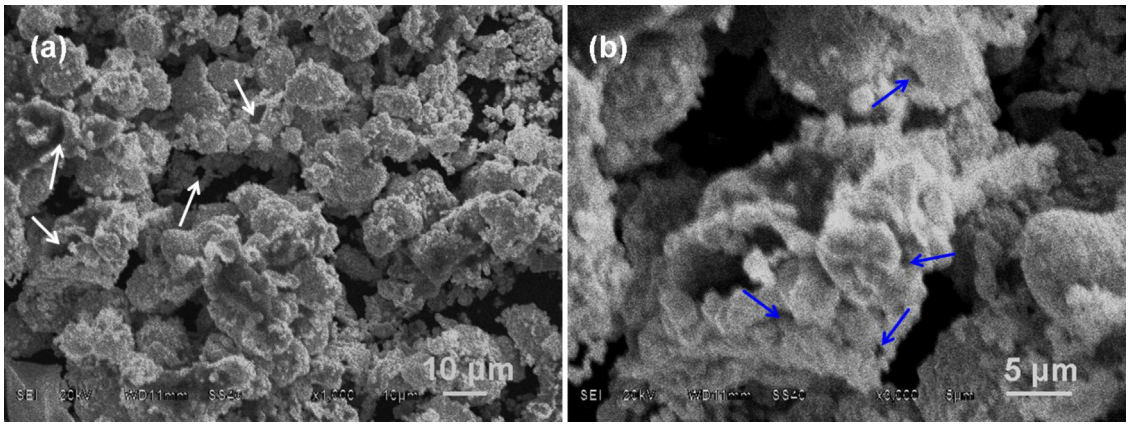

Fig. 4. SEM images of AgCl@Ag HAs. (For interpretation of the references to color in text, the reader is referred to the web version of the article.)

the chemical etching process. From the cracked parts of the architectures, their interiors can be clearly observed (indicated by white arrows in Fig. 4a). The close observation of the SEM image (Fig. 4b) revealed that the surfaces of the AgCl@Ag architectures were rather rough so that the polyhedron edges and facets were difficult to identify, which significantly differs from those of the Ag_2CO_3 template (Fig. 1a). From a broken architecture as shown in Fig. 4b, the hollow cavity can be clearly visible, where the shells of the hollow architectures were constructed by numerous aggregated tiny particles with a unique porous structure in the shells (indicated by blue arrows in Fig. 4b). Unfortunately, we failed to obtain TEM images of the AgCl@Ag products, because the particles were destroyed by the high-energy electron beam during the measurement.

Based on the above experimental observations, we proposed the formation process of AgCl@Ag HAs. As schematically illustrated in Fig. 5, the uniform Ag_2CO_3 architectures could be easily obtained by means of adding an aqueous solution of $NaHCO_3$ dropwise into an aqueous solution of $AgNO_3$. These Ag_2CO_3 architectures then serve as sacrificial templates and reservoir of silver ions by adding the reactive reagent NH_4Cl for the subsequent reaction. The hydrolysis of NH_4Cl leading to H^+ in aqueous solution occurs preferentially around the alkaline carbonate Ag_2CO_3 architectures. Simultaneously, the Ag_2CO_3 architectures are acidic etching and immediately transformed to AgCl ($2NH_4Cl + Ag_2CO_3 + H_2O \rightarrow 2AgCl + CO_2 + 2NH_4OH$), wherein the formed AgCl could be partially converted into AgCl@Ag in situ by ambient light [25–27]. Finally, a hollow structure emerges as a result of outward flow of Ag^+ ions when the Ag_2CO_3 template is continuously consumed. Notably, the acidic etching of the carbonate templates would induce the release of a mass of gases (such as CO_2) from the interior of architectures, thus leading to a remarkable porosity left inside the particles.

The optical properties of the AgCl@Ag HAs were characterized by UV–vis diffuse reflectance spectroscopy (DRS). Fig. 6 shows the UV–vis DRS of the AgCl@Ag products. The AgCl@Ag HAs exhibited strong characteristic absorption of AgCl in the range of 200–350 nm, in which the two peaks around 240 and 280 nm should be ascribed

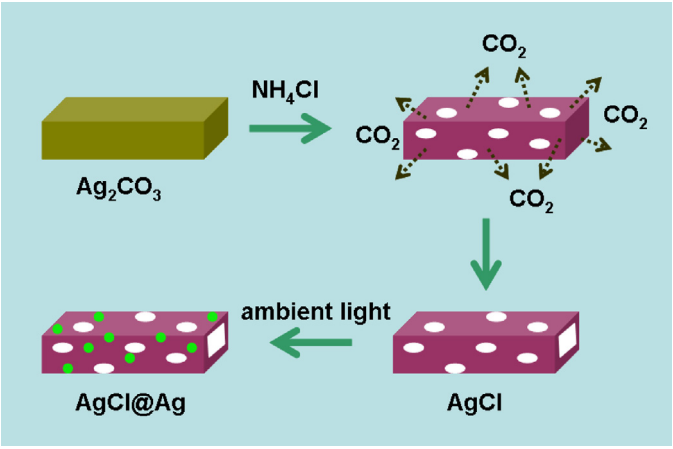

Fig. 5. Schematic diagram of the formation mechanism of hierarchical porous AgCl@Ag HAs.

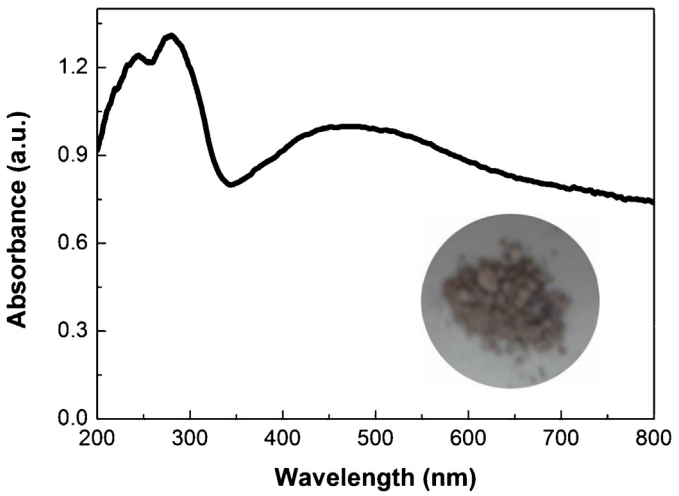

Fig. 6. UV–vis diffuse reflectance spectrum and the photograph (inset) of the AgCl@Ag HAs. (For interpretation of the references to color in text, the reader is referred to the web version of the article.)

to the direct and indirect exciton transitions of AgCl, respectively [28]. In contrast, prominent absorption region in the range from 400 to 700 nm is interestingly found, which is attributed to the surface plasmon resonance (SPR) of Ag NPs. Consistent with the DRS results, the color of the AgCl@Ag HAs is pale red (inset in Fig. 6), much different from the white-colored AgCl. This distinct absorption in visible region is expected to achieve an enhanced light-harvesting efficiency for high performance visible light photocatalysis.

The photocatalytic activity of the AgCl@Ag products was evaluated by the degradation of MO under visible light irradiation ($\lambda > 420$ nm). Fig. 7a shows the relative concentration (C/C_0) of MO as a function of time, where C is the concentration of MO at the irradiation time t and C_0 is the initial concentration of MO solution before irradiation. The photocatalytic measurements were carried out by using different photocatalysts as well as the control experiments. After visible light irradiation for 12 min, no observation of the photolysis of MO in the absence of the photocatalyst reflects the MO was quite stable under visible light irradiation. The metallic Ag NPs alone show negligible photodegradation of MO under visible light irradiation, which not only implies the poor photoreactivity of metallic Ag, but also excludes the possible surface plasmon induced localized heating effect in catalytic system [29,30]. Also, commercial P25 as a reference showed almost no photocatalytic activity toward the degradation of MO under identical conditions. However, after 12 min of degradation under visible light irradiation, 85% of MO was photocatalytically degraded on the AgCl@Ag HAs, indicating their high photocatalytic efficiency. Fig. 7b shows the temporal evolution of spectral changes of MO solution photodegraded by the AgCl@Ag HAs. It is shown that MO can be rapidly decomposed in the presence of our AgCl@Ag HAs photocatalyst under visible light irradiation. For comparison, we also conducted MO photodegradation experiments on our previously reported AgCl@Ag solid architectures (denoted as AgCl@Ag SAs, Fig. 9b) with a similar molar ratio of AgCl:Ag (12.2:1) to AgCl@Ag HAs [20] and Ag@AgCl with different situation of two components from AgCl@Ag HAs (denoted as Ag@AgCl, Fig. 9b). We found the photocatalytic activity of AgCl@Ag HAs to be much higher than that of AgCl@Ag SAs and Ag@AgCl (Fig. 7a). The photodegradation processes could

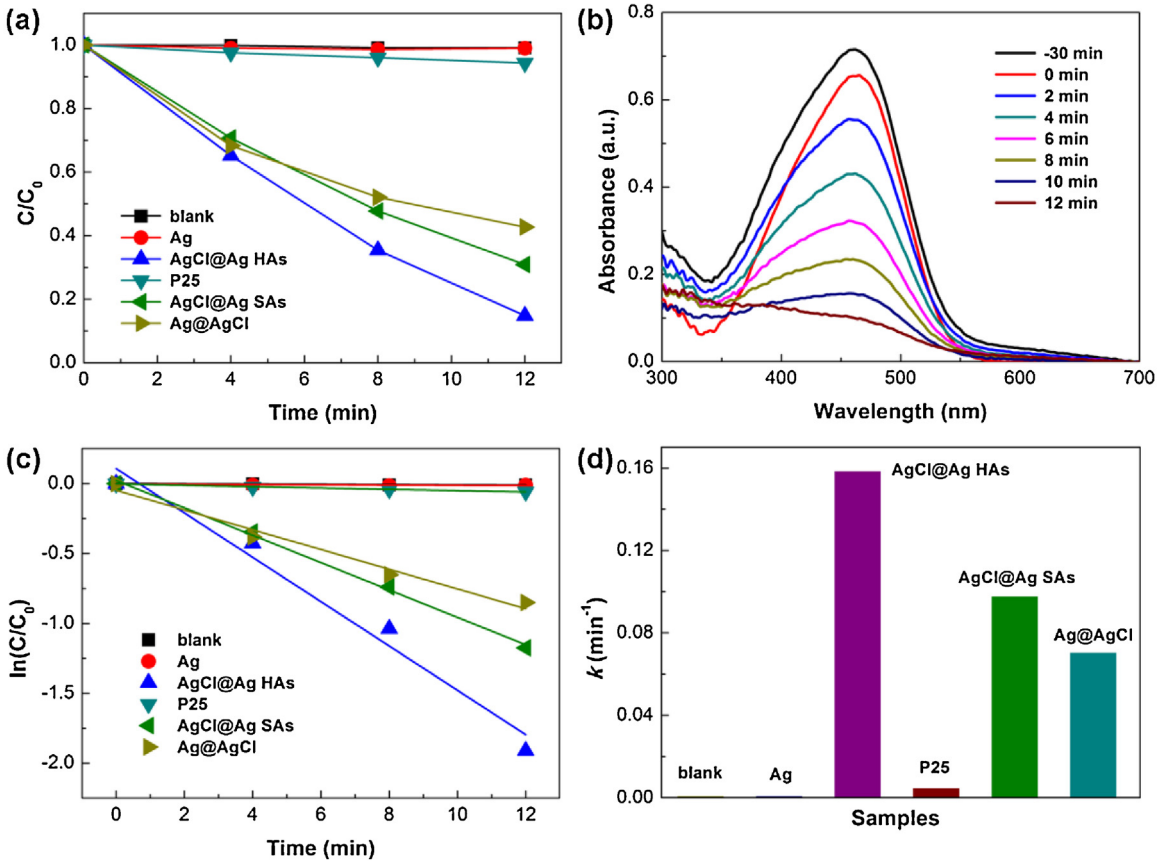

Fig. 7. (a) Photocatalytic performances of the investigated photocatalysts for the photodegradation of MO under visible light irradiation ($\lambda > 420$ nm). (b) UV–vis spectral evolution of MO as a function of irradiation time over AgCl@Ag HAs. (c) Kinetic linear simulation curves and (d) kinetic constants of the investigated photocatalysts for the photodegradation of MO under visible light irradiation ($\lambda > 420$ nm).

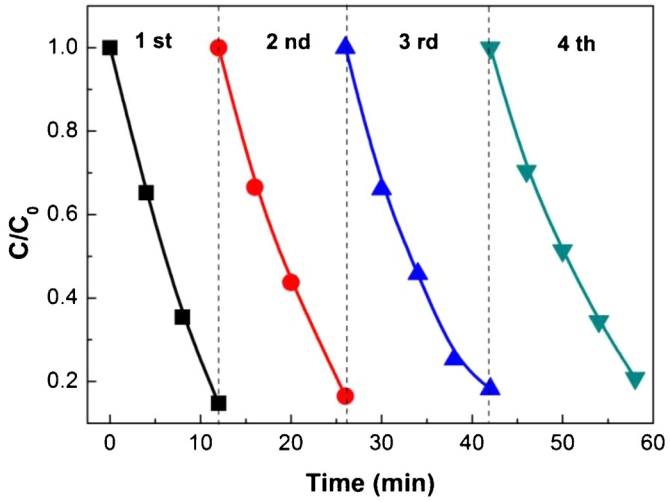

Fig. 8. Recycling test on AgCl@Ag HAs for MO photodegradation under visible light irradiation (λ > 420 nm).

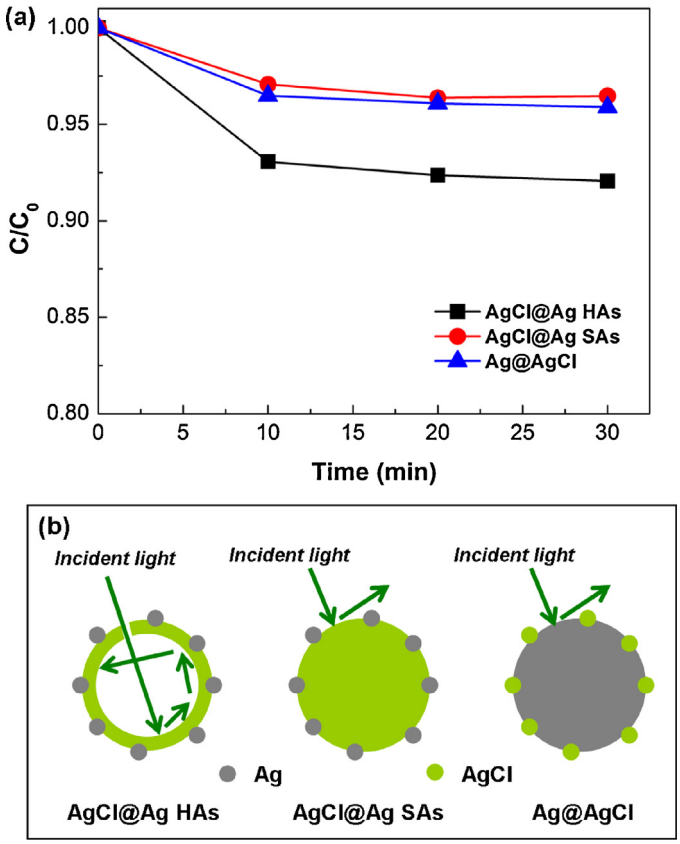

Fig. 9. (a) Time profiles of adsorption of MO over different photocatalysts in the dark. (b) Schematic illustration of structure model and light absorbance model of different photocatalysts.

be fitted to pseudo-first-order kinetics (Fig. 7c), $\ln(C/C_0) = kt$, where C is the concentration of the MO at time t, C_0 is the initial concentration of the MO solution, and the slope k is the apparent reaction rate constant. The apparent rate constants (Fig. 7d) for the AgCl@Ag HAs, AgCl@Ag SAs and Ag@AgCl were evaluated as 0.1586, 0.0979 and 0.0706 min^{-1}, respectively. The photocatalytic activity of AgCl@Ag HAs was thus about 1.6 times as high as that of AgCl@Ag SAs and about 2.2 times that of Ag@AgCl, indicating enhanced photocatalytic performance of our AgCl@Ag HAs. Moreover, the stability of our AgCl@Ag HAs plasmonic photocatalysts was evaluated in terms of performing the MO photodegradation repeatedly four times. As shown in Fig. 8, after four recycles for the photodegradation of MO, the catalyst does not exhibit any significant loss of activity, indicating the catalysts' good stability for photocatalysis. Since silver-based compounds are common photosensitive materials, it is possible that the photogenerated electrons reduce Ag^+ in AgCl to metallic Ag, such a phenomenon has already been reported previously in Ag_2O [31], $AgSbO_3$ [32] and Ag_3PO_4 [33] as photocatalysts. Therefore, we further collected the reused photocatalyst after photoreaction to check the photostability of AgCl@Ag HAs. The composition and XRD pattern of the AgCl@Ag HAs does not show significant variation after recycle experiments (see Figs. S1 and S2 in Supplementary data). These results confirm that the AgCl@Ag HAs are stable under our experimental conditions, consistent with previously reported observations [14,18,26,34].

It is generally accepted that the porous hollow structure could provide abundant active sites available and multiple accessible channels for diffusion and transport of organic molecules, which is beneficial to improving the adsorption and photocatalytic efficiency. To well understand the high photoreactivity of the AgCl@Ag HAs, we further carefully examined the adsorption of MO over AgCl@Ag HAs, AgCl@Ag SAs and Ag@AgCl. The results (Fig. 9a) unambiguously reveal that the AgCl@Ag HAs possesses higher MO adsorption efficiency than AgCl@Ag SAs or Ag@AgCl. Furthermore, the hollow structure allow multiple reflections of light within the hollow cavity of AgCl@Ag HAs, thus is also favorable for the efficient utilization of the light source (Fig. 9b), which might be responsible for the superior photocatalytic performance of our AgCl@Ag HAs as well.

In the photocatalysis process for the degradation of organic pollutants, photogenerated electron–hole pairs (e^-–h^+) that migrate to the surface of catalysts could induce active species involved in the photoreaction. Therefore, it is of great importance to investigate the main active species in the photocatalytic process to further insight into the underlying photocatalytic mechanism. The primary active species in the photocatalytic process could be detected through the trapping experiments of radicals and holes by using different scavengers, such as isopropyl alcohol for hydroxyl radical, and sodium oxalate or EDTA for hole. As shown in Fig. 10, the photocatalytic degradation of MO over AgCl@Ag HAs was not affected by the addition of isopropyl alcohol. On the contrary, the photocatalytic activity of AgCl@Ag HAs was greatly suppressed with the addition of sodium oxalate or EDTA. On the other hand, considering that the superoxide radical could be generated through a direct reaction of the photoinduced electron with molecular oxygen adsorbed on the surface of photocatalyst, an anaerobic experiment was further conducted to elucidate the role of molecular oxygen in our AgCl@Ag HAs catalytic system. As shown in Fig. 10, slight change of the MO photodegradation rate was observed, implying that molecular oxygen played a minor role therein. This result suggested that the photogenerated holes should be the main active species for the degradation of MO on AgCl@Ag HAs.

On the basis of the above results, we can analyze the origin of the high photoreactivity of the AgCl@Ag HAs. It is widely accepted that energy transfer mechanisms during plasmonic photocatalysis process generally includes: (i) hot charge transfer, (ii) surface plasmon induced localized heating effect, and (iii) local electromagnetic field enhancement [35]. The above observed negligible photoreaction of bare metallic silver unambiguously rules out the plasmon heating effect. Also, the near-field electromagnetic enhancement normally is observed for the photocatalytic system with an overlap between the spectra of the illumination source, plasmon resonance and semiconductor absorbance. However, the AgCl cannot adsorb visible light under the present conditions (visible light, λ > 420 nm), because it has a direct bandgap of 5.15 eV (241 nm) and an indirect

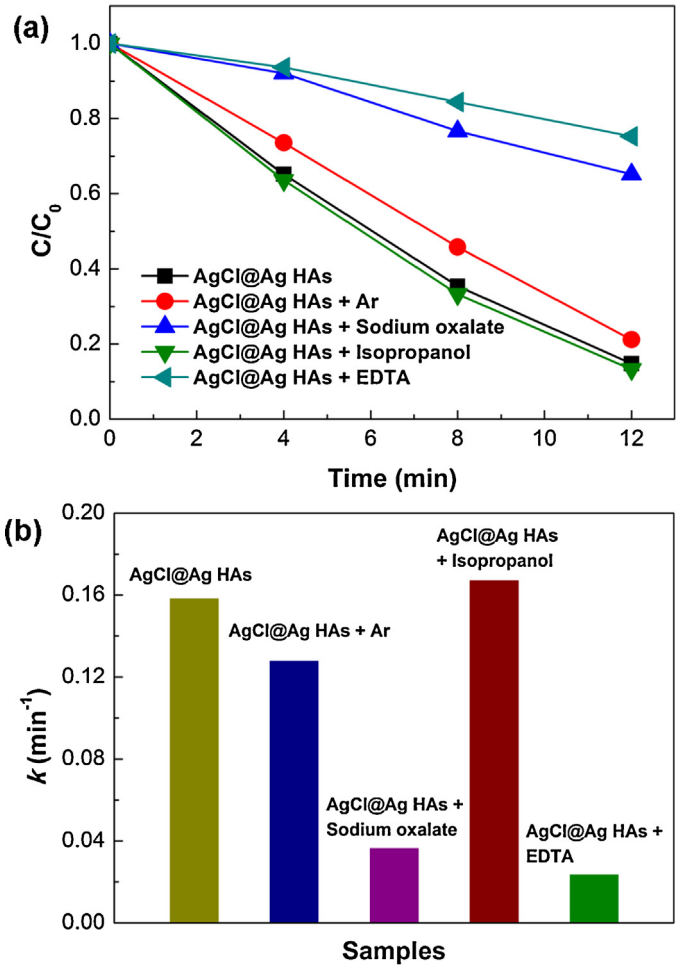

Fig. 10. (a) Photocatalytic performances and (b) kinetic constants of the AgCl@Ag HAs for the photodegradation of MO under visible light irradiation ($\lambda > 420$ nm) in the presence of trapping systems.

bandgap of 3.25 eV (382 nm) [36]. In this regard, it is reasonable to believe that the SPR-mediated hot charge transfer mechanism is mainly contributed to the enhanced photocatalytic performance of the AgCl@Ag HAs. The plasmonically photocatalytic process can be understood qualitatively by the schematic band diagram of the AgCl@Ag shown in Fig. 11. A Schottky junction is created at the Ag–AgCl interface, leading to charge transfer from the AgCl to the Ag NPs and producing a potential barrier of 0.8 eV [37]. Upon visible light irradiation, surface plasmons are generated in the excited Ag NPs and rapidly decay to induce several hot electrons. These

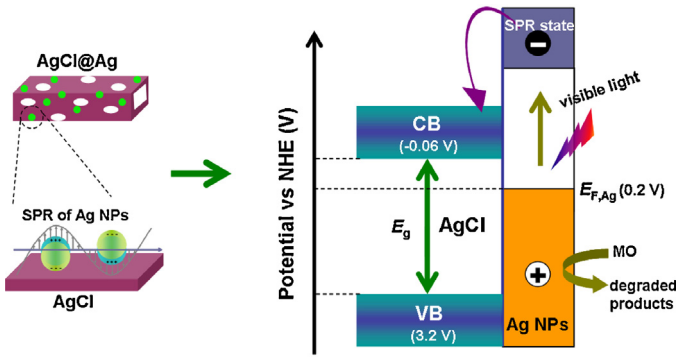

Fig. 11. Schematic illustration of the photocatalytic process for AgCl@Ag HAs under visible light irradiation.

hot electrons transiently occupy normally empty states in the CB of Ag above the Fermi energy. A fraction of SPR-mediated energetic electrons are injected to the CB of AgCl, causing a temporary positively charged metal surface. Notably, as the CB energy level of AgCl (−0.06 V vs NHE) is more negative than the potential of O_2/HO_2 (O_2/HO_2: −0.046 V vs NHE), these electrons could reduce oxygen to HO_2 through the single-electron reaction ($O_2 + e^- + H^+ \rightarrow HO_2$) [31,38]. As a result, the energetic positive charge on the surface of metallic Ag NPs can then contribute to the oxidation of organic dyes, which is remarkably consistent with the results of trapping experiment of active species. It is generally accepted that direct contact between organic molecules and photocatalysts is a prerequisite for the direct photohole oxidation [39]. As aforementioned, a hollow porous structure can improve the adsorption of MO over AgCl@Ag HAs by providing more active sites and thus enable the holes to more effectively oxidize MO. This should account for the enhanced photoreactivity of AgCl@Ag HAs.

4. Conclusions

In summary, we have demonstrated a facile and efficient acidic etching process for the preparation of hierarchical porous AgCl@Ag hollow architectures by using sacrificial Ag_2CO_3 as template at room temperature. Moreover, the as-synthesized AgCl@Ag HAs exhibit more efficient visible-light-driven photocatalytic activities for the degradation of MO as compared to the counterparts AgCl@Ag SAs under visible light irradiation. The rate constant for the degradation of MO photocatalyzed by AgCl@Ag HAs was 1.6 times that of AgCl@Ag SAs. The enhanced photocatalytic activity could be attributed to the hierarchical hollow morphology and unique porous structure, which facilitates the increased adsorption and enhanced light-harvesting efficiency. It is reasonable to believe that our AgCl@Ag HAs will be a promising candidate for solar energy conversion.

Acknowledgements

This work was supported by the National Natural Science Foundation of China (21103141 and 21207108), the Applied Basic Research Program of Sichuan Provincial Science and Technology Department (2011JYZ019) and the Research Foundation of CWNU (12B018).

Appendix A. Supplementary data

Supplementary data associated with this article can be found, in the online version, at http://dx.doi.org/10.1016/j.apcatb.2013.05.053.

References

[1] X. Chen, L. Liu, P.Y. Yu, S.S. Mao, Science 331 (2011) 746–750.
[2] X. Chen, S. Shen, L. Guo, S. Mao, Chemical Reviews 110 (2010) 6503–6570.
[3] X. Chen, S. Mao, Chemical Reviews 107 (2007) 2891–2959.
[4] Z. Wang, J. Song, Science 312 (2006) 242–246.
[5] C. Liu, Q. Kuang, M.-S. Jin, J.-W. Zhang, X.-G. Han, Z.-X. Xie, L.-S. Zheng, Nanoscale 5 (2013) 1793–1796.
[6] J.H. Pan, X. Zhang, A.J. Du, D.D. Sun, J.O. Leckie, Journal of the American Chemical Society 130 (2008) 11256–11257.
[7] H. Cheng, B. Huang, Y. Liu, Z. Wang, X. Qin, X. Zhang, Y. Dai, Chemical Communications 48 (2012) 9729–9731.
[8] D. Chen, J. Ye, Advanced Functional Materials 18 (2008) 1922–1928.
[9] J. Zhu, Z. Yin, D. Yang, T. Sun, H. Yu, H.E. Hoster, H.H. Hng, H. Zhang, Q. Yan, Energy & Environmental Science 6 (2013) 987–993.
[10] K. Ren, K. Zhang, J. Liu, H. Luo, Y. Huang, X. Yu, CrystEngComm 14 (2012) 4384–4390.
[11] X. Chen, J. Liu, H. Wang, Y. Ding, Y. Sun, H. Yan, Journal of Materials Chemistry A 1 (2013) 877–883.
[12] N. Zhang, S. Ouyang, T. Kako, J. Ye, Chemical Communications 48 (2012) 9894–9896.

[13] X. Li, R. Huang, Y. Hu, Y. Chen, W. Liu, R. Yuan, Z. Li, Inorganic Chemistry 51 (2012) 6245–6250.
[14] P. Wang, B. Huang, X. Qin, X. Zhang, Y. Dai, J. Wei, M.-H. Whangbo, Angewandte Chemie International Edition 47 (2008) 7931–7933.
[15] C. An, R. Wang, S. Wang, X. Zhang, Journal of Materials Chemistry 21 (2011) 11532–11536.
[16] X. Hu, C. Hu, T. Peng, X. Zhou, J. Qu, Environmental Science & Technology 44 (2010) 7058–7062.
[17] C. An, J. Wang, W. Jiang, M. Zhang, X. Ming, S. Wang, Q. Zhang, Nanoscale 4 (2012) 5646–5650.
[18] C. An, S. Peng, Y. Sun, Advanced Materials 22 (2010) 2570–2574.
[19] M. Zhu, P. Chen, M. Liu, Journal of Materials Chemistry 21 (2011) 16413–16419.
[20] J. Jiang, L. Zhang, Chemistry – A European Journal 17 (2011) 3710–3717.
[21] L. Ai, H. Yue, J. Jiang, Nanoscale 4 (2012) 5401–5408.
[22] L. Ai, J. Jiang, Journal of Materials Chemistry 22 (2012) 20586–20592.
[23] L. Ai, J. Jiang, Nanotechnology 23 (2012), 495601 (9 pp.).
[24] D. Chen, S.H. Yoo, Q. Huang, G. Ali, S.O. Cho, Chemistry – A European Journal 18 (2012) 5192–5200.
[25] M. Zhu, P. Chen, W. Ma, B. Lei, M. Liu, ACS Applied Materials & Interfaces 4 (2012) 6386–6392.
[26] M. Zhu, P. Chen, M. Liu, ACS Nano 5 (2011) 4529–4536.
[27] M. Zhu, P. Chen, M. Liu, Langmuir 28 (2012) 3385–3390.
[28] R. Dong, B. Tian, C. Zeng, T. Li, T. Wang, J. Zhang, Journal of Physical Chemistry C 117 (2013) 213–220.
[29] P.L. Redmond, L.E. Brus, Journal of Physical Chemistry C 111 (2007) 14849–14854.
[30] W.H. Hung, M. Aykol, D. Valley, W. Hou, S.B. Cronin, Nano Letters 10 (2010) 1314–1318.
[31] X. Wang, S. Li, H. Yu, J. Yu, S. Liu, Chemistry – A European Journal 17 (2011) 7777–7780.
[32] W. Liu, X. Liu, Y. Fu, Q. You, R. Huang, P. Liu, Z. Li, Applied Catalysis B: Environmental 123–124 (2012) 78–83.
[33] W. Wang, B. Cheng, J. Yu, G. Liu, W. Fan, Chemistry – An Asian Journal 7 (2012) 1902–1908.
[34] H. Zhang, X. Fan, X. Quan, S. Chen, H. Yu, Environmental Science and Technology 45 (2011) 5731–5736.
[35] S. Linic, P. Christopher, D.B. Ingram, Nature Materials 10 (2011) 911–921.
[36] S. Glaus, G. Galzaferri, Photochemical & Photobiological Sciences 2 (2003) 398–401.
[37] Y. Tang, Z. Jiang, J. Xing, A. Li, P.D. Kanhere, Y. Zhang, T.C. Sum, S. Li, X. Chen, Z. Dong, Z. Chen, Advanced Functional Materials (2013), http://dx.doi.org/10.1002/adfm.201203379.
[38] X. Wang, S. Li, Y. Ma, H. Yu, J. Yu, Journal of Physical Chemistry C 115 (2011) 14648–14655.
[39] G. Dong, L. Zhang, Journal of Materials Chemistry 22 (2012) 1160–1166.